HHS Public Access

Author manuscript

IEEE Trans Ultrason Ferroelectr Freq Control. Author manuscript; available in PMC 2015 October 19.

Published in final edited form as:

IEEE Trans Ultrason Ferroelectr Freq Control. 2015 February ; 62(2): 319–328. doi:10.1109/TUFFC.2014.006728.

Real-Time Integrated Photoacoustic and Ultrasound (PAUS) Imaging System to Guide Interventional Procedures: *Ex Vivo* Study

Chen-Wei Wei, **Thu-Mai Nguyen**, **Jinjun Xia**, **Bastien Arnal**, **Emily Y. Wong**, **Ivan M. Pelivanov**, and **Matthew O'Donnell**

Department of Bioengineering, University of Washington, Seattle, WA

Chen-Wei Wei: cwwei28@uw.edu

Abstract

Because of depth-dependent light attenuation, bulky, low-repetition-rate lasers are usually used in most photoacoustic (PA) systems to provide sufficient pulse energies to image at depth within the body. However, integrating these lasers with real-time clinical ultrasound (US) scanners has been problematic because of their size and cost. In this paper, an integrated PA/US (PAUS) imaging system is presented operating at frame rates >30 Hz. By employing a portable, low-cost, low-pulse-energy (~2 mJ/pulse), high-repetition-rate (~1 kHz), 1053-nm laser, and a rotating galvo-mirror system enabling rapid laser beam scanning over the imaging area, the approach is demonstrated for potential applications requiring a few centimeters of penetration. In particular, we demonstrate here real-time (30 Hz frame rate) imaging (by combining multiple single-shot sub-images covering the scan region) of an 18-gauge needle inserted into a piece of chicken breast with subsequent delivery of an absorptive agent at more than 1-cm depth to mimic PAUS guidance of an interventional procedure. A signal-to-noise ratio of more than 35 dB is obtained for the needle in an imaging area 2.8 × 2.8 cm (depth × lateral). Higher frame rate operation is envisioned with an optimized scanning scheme.

I. Introduction

Photoacoustic (PA) imaging complements clinical ultrasound (US) by adding optical absorption as a contrast mechanism at spatial resolutions comparable to US for penetration depths up to a few centimeters [1]–[4]. Using the same transducers and imaging electronics, it can provide molecular information absent from US images. US-guided PA imaging can have several clinical applications related to imaging the vasculature (exploiting hemoglobin contrast) [5]; detecting molecularly-targeted, nanoscale contrast agents [6]–[10]; and guiding interventional procedures [11]. An integrated scan format in which PA/US (PAUS) image frames are interleaved at real-time rates is needed for optimal translation of this technology to the clinic.

The first three authors made equal contribution to this work.

I. M. Pelivanov is also with the International laser Center, Moscow State University, Moscow, Russian Federation.

Integrated PAUS systems have been developed as a research tool [12]–[14]. Typically, high-pulse-energy (tens to hundreds of millijoules per pulse) Q-switched lasers are required to produce high-SNR PA signals induced by nanosecond pulses. However, these laser sources are generally not cost effective, massive (usually >1 m long with a bulky power unit), and hard to maintain. In addition, their low pulse repetition frequency (PRF; usually <20 Hz) can severely limit image frame rates for real-time operation, hindering integration of photoacoustics with a real-time commercial US scanner for clinical applications. To facilitate clinical translation of interleaved PAUS imaging, we propose to use a low-cost (<30 000 USD) and portable (<30 cm in any dimension) laser integrated with a commercial US scanner, appropriate for several clinical applications.

Portable fiber-amplified semiconductor-based lasers and laser diode-pumped Q-switched lasers are relatively inexpensive and output nanosecond pulses with repetition rates up to several hundreds of kilohertz. However, their single pulse energies are quite low, in most cases from hundreds of microjoules up to a few millijoules. Such low energies distributed over the entire image volume cannot generate PA signals with acceptable SNR for single-pulse operation. To maintain acceptable optical fluence (energy per unit area) for high-SNR measurements, the beam must be focused to a small spot. This means the lateral extent of the image is quite limited. In addition, optical scattering is very strong for most biological tissues in the visible and near-infrared optical wavelength range, limiting light penetration, especially for a small beam spot.

The SNR can be improved by averaging. However, the SNR improvement from averaging only increases as the square root of the number of pulses, and the PRF is limited by the acoustic time-of-flight to avoid range ambiguities (i.e., sources from multiple ranges delivering PA signals to the ultrasound array at the same time). For example, to image a 1-cm region, the laser pulse repetition interval (PRI) should be larger than the acoustic propagation time,

$$\mathrm{PRI}=1/\mathrm{PRF}\geq\frac{\mathrm{imaging\ \ range}}{\mathrm{sound\ \ velocity}}=\frac{1\mathrm{cm}}{1540\mathrm{m/s}}. \quad (1)$$

The maximum PRF is, therefore, 154 kHz. Furthermore, laser safety regulations (maximum average power of 1 W/ cm^2 [15]) also limit the repetition rate for a given laser fluence. For example, the maximum fluence allowed for a 1-kHz laser is 1 mJ/cm^2, a value producing low optical intensities deep inside the body. Therefore, there is a tradeoff between SNR (related to laser fluence) and image frame rate (related to PRF).

Here, we propose to manage these limitations by combining multiple laser shots to scan over the area of interest. A high-repetition-rate (~1 kHz), low-energy (~a few millijoules) laser enables rapid scanning. PA signals induced by each laser shot are recorded to form a sub-frame of RF data. PA sub-images corresponding to the narrow beam sub-frame can be reconstructed to show regional information near the laser scanning spot. The final PA image covering the complete scan area is synthetically reconstructed by combining all RF sub-frames. The effectiveness of this method was demonstrated conceptually in a previous study [16], [17] in which synthetic PA imaging from multiple narrow beams produced an SNR

similar to that from a conventional large-area, high-pulse-energy single laser shot at imaging depths of 1 to 2 cm. In this paper, we expand on the previous work to present a real-time interleaved PAUS system with a frame rate of 30 Hz using a very compact, low-cost diode-pumped laser.

Near real-time or real-time PA imaging has also been reported. Razansky and Ntziachristos developed and built a PA system for small animal imaging with a 10-Hz laser [18]–[20]. Recently, the system was commercialized (iThera Medical, Munich, Germany) [21] with a 100-Hz laser. A disadvantage of that system is that it is bulky and expensive, mostly because of the large size and high cost of the laser used. Wang *et al.* reported 40-Hz frame rate PA microscopy at a few millimeters depth using a 30-kHz laser with a voice-coil stage to scan both the light beam and a single-element US probe [22]. The scanning approach has also been published for PA imaging with a galvanometer scanner [23], or with a MEMS mirror inside a single-element US transducer to scan the laser beam [24]. However, the systems [22], [23] are developed to achieve optical spatial resolution for PA microscopy applications with very limited imaging depth (<1 cm) and field of view, not appropriate for clinical applications requiring imaging at centimeters depth. For [24], real-time deep imaging is impossible due to the small scan region (1 × 1 mm), the slow (10 Hz) laser used, and the single-element transducer requiring mechanical scanning to cover a wide region. Also, none of these systems incorporate an US frame, limiting their use for US-guided applications [18]–[24].

Alquasemi *et al.* reported interleaved PAUS imaging using FPGA modules [13]. Combining laser systems with a commercial US scanner for integrated PAUS imaging has been published by many groups [25]–[27]. Commercial integrated PAUS imaging products are also available, such as Vevo LAZR (FujiFilm VisualSonics Inc., Toronto, Canada) providing 2-D/3-D co-registered PAUS images for visualizing small animal anatomy and analyzing function *in vivo*. Unfortunately, the frame rate of these systems is less than 30 frames/s, limited by the slow and bulky laser used.

In our approach, several US pulse–echo beams are formed close to the scanning laser beam location after each laser firing and PA sub-frame recording, rather than interleaving one full PA frame and one full US frame. There are two benefits of interleaving US beams between PA sub-frames (laser firings): 1) both US and PA information are acquired at the same spatial location; this is especially important for imaging moving objects or monitoring fast-changing dynamics, and 2) the dead-time between laser firings (tens of microseconds PA recording for centimeters range versus the millisecond PRI for a kilohertz laser) is fully utilized, increasing the frame rate because US pulse– echo recordings don’t have to wait until all PA recordings are finished. To the best of our knowledge, this is the first report of an interleaved PAUS imaging system for deep imaging (up to a couple of centimeters) with a frame rate >30 Hz.

In this study, we investigate the potential of using the proposed PAUS imaging system for a clinical application where co-registered PAUS is needed to provide real-time and precise monitoring with high-contrast images: guidance of needle insertion and therapeutic injection. US image-guided needle monitoring has been commonly used in many clinical

applications such as biopsy in prostate [28], and breast [29], and therapeutic agent injection [30]. Unfortunately, the quality of the US image is directly related to the orientation of the needle relative to the scan direction of the real-time image because the primary signal from a needle is the specular reflection from its surface. In many cases, proper orientation is problematic and tracking precision is lost because of the poor US contrast and additional artifacts associated with the needle. In addition, background scattering also degrades contrast to distinguish the needle and injected agents inside turbid tissue, limiting the precision of the biopsy and injection procedure.

In contrast, the PA signal from the needle is much less dependent on the orientation of the light source and less sensitive to needle-transducer orientation. The reason is that the needle is a cylindrical acoustic source in PA imaging, with directivity pattern oriented in the direction covered by the transducer imaging field. In contrast, the needle is a reflector in the US mode, which usually scatters the probe US beam in a direction different from that of the incident US beam. As a result, PA is less sensitive to transducer-target orientation (one-way propagation), compared with US (round-trip propagation). PA needle guidance can potentially be much more robust than US guidance, especially for non-expert users. Also, PA imaging exhibits higher contrast (based on optical absorption) to monitor injected exogenous agents because of the speckle-free background.

Ex vivo imaging experiments of needle insertion into chicken tissue and injection of an absorptive agent into that tissue were performed.

II. Materials and Methods

A. Experimental Setup and Sample Preparation

Fig. 1 shows a schematic of the PAUS integrated setup. A US linear array (AT8L12-5 50 mm, Broadsound Corp., Hsinchu, Taiwan; central frequency 9 MHz, bandwidth 5 to 12 MHz, 256 elements, 195 μm pitch, elevation focus 20 mm) was used for both US pulse–echo imaging and PA signal reception. In further descriptions, axial and lateral will refer to directions respectively parallel and perpendicular to the US probe beam axis.

A diode-pumped laser (TECH-1053 specific, Laser-Export Co. Ltd., Moscow, Russia) delivered 10-ns pulses with a pulse energy of 1.9 mJ at a wavelength of 1053 nm with a 2.8-mm beam diameter, resulting in a fluence of 31 mJ/cm^2 at the sample surface. This fluence is well below safety limits, 100 mJ/cm^2, at this wavelength [15]. The advantage of this laser is its compact size (physical dimensions are 215 × 70 × 40 mm) and low cost (20 000 USD). The maximum pulse repetition rate is 100 kHz, with maximum output pulse energy of about 2.2 mJ at 1 kHz. The beam was directed to a scanning galvo-mirror (GVS001, Thorlabs Inc., Newton, NJ) from the laser source. The mirror angle was varied between −1° and +1° using a sinusoidal waveform delivered by a function generator (AFG 3252, Tektronix Inc., Beaverton, OR). At a distance of 30 cm from the target, such an angular range yields a lateral imaging range of ~1 cm. There are two constraints that must be addressed when choosing the illumination condition: 1) the laser fluence should be under 100 mJ/ cm^2 (at 1053 nm wavelength) [15] for a single laser firing, and 2) the average power should be under 1 W/cm^2 [15] at every sample point. Consequently, to meet real-time frame rates (>30 Hz),

the fluence is limited to 33 mJ/cm^2 (1 W/cm^2/30 Hz) because the laser spot returns to the same position every 1/30 s (time of the whole scanning cycle). A tradeoff between SNR (related to fluence) and frame rate was considered in designing the illumination sequence. In summary, a 30-Hz frame rate (mirror scan rate) was set, with 24 scanning beams over a 1 cm range and a laser pulse repetition rate set to 720 Hz. The axial imaging range was set to 2.8 cm. Both laser beam and US probe were placed on the top of the sample and aligned so that the incident plane of the light and the probe imaging plane intersect at the target depth. The laser beam was tilted by about 45° with respect to the US probe.

As an example of the potential clinical applicability of this system, here we demonstrate needle guidance within a piece of chicken breast (~3 cm in thickness). The chicken breast phantom was surrounded by a 10% acoustically and optically transparent gelatin shell (1-cm thickness) for US coupling (see Fig. 1). An 18-gauge needle (1.27-mm outer diameter, 18G1, Becton Dickinson & Co., East Rutherford, NJ) was mounted on a linear stage (TLA60A, Zaber Technologies Inc., Vancouver, BC, Canada) for insertion laterally into the chicken breast with a tilt angle of ~20°. The depth is up to 12 mm inside the biological tissue (chicken breast). With an estimated light-tissue incident angle of 45°, the light propagation path into the tissue was close to 17 mm. To demonstrate the real-time ability of our system, we imaged both the insertion of the needle as well as the injection through the inserted needle of an ink solution (44011, Higgins Ink, Leeds, MA), mimicking delivery of a therapeutic agent such as a small-molecule drug. The ink solution had an optical absorption coefficient of 20 cm^{-1} at 1053 nm.

B. System Block Diagram

A block diagram of the system is presented in Fig. 2. A programmable ultrasound scanner (Vantage, Verasonics Inc., Redmond, WA) is used for all image data acquisition and reconstruction. The system is operated using Matlab (The MathWorks Inc., Natick, MA). The function generator is used to synchronize all operations (i.e., laser firings, PA signal recording, and mirror position). In addition to sending a sine-wave signal to drive the scanning mirror, it sends triggers to the laser and the Verasonics scanner simultaneously to synchronize PA signal recording with each laser firing. During one period of the sine wave, multiple laser firings (i.e., multiple trigger signals) are emitted, covering the entire lateral imaging range (~1 cm). After each laser firing and PA signal recording, several US pulse–echo beams are formed. The transmit US pulse has a center frequency of 7.8 MHz, and the sampling frequency on receive is 31.25 MHz with a bandwidth of 2 times the center frequency. Additional details about interleaved PAUS recoding is provided in the next section.

To maximize frame rate, a large data set (corresponding to several mirror cycles) is acquired and then transferred at once, while the next data set is being acquired. This ensures continuous acquisition (see details in the next section).

C. System Detailed Timing Diagram

The detailed timing of the acquisition for one data set is shown in Fig. 3. The system runs continuously by repeating this acquisition set.

The number of mirror cycles constituting one data set, i.e., *n*, is an input from the control program and is determined by the maximum amount of data that can be transferred at once by the hardware of the Verasonics scanner. For each mirror cycle, there are 24 laser firings for PA receives (128 channels for each laser firing). Each laser firing/PA receive was followed by 6 full beams of pulse–echo US focused at 6 different adjacent lateral locations. Laser firings are preceded by adding a flush time (no operation, 100 μs in current setup) to prevent US emissions from interfering with PA signal recording. This pattern is repeated until one mirror cycle is completed, allowing the laser beam to cover the entire lateral imaging range, and leads to:

- One integrated PA frame, resulting from a total of 24 laser firings at a 720 Hz repetition rate (i.e., 24 single-shot sub-images);
- One integrated US frame consisting of 144 US pulse–echo focused beams swept laterally across the imaging range, similar to conventional B-mode US imaging.

The Verasonics data transfer time from the front end to the host computer memory is determined by a transfer rate of 6600 MB/s and also includes a few milliseconds (typically 5 ms) overhead for each transfer. To reduce the number of transfers, a large data set is acquired and then transferred all at once. Each data set therefore corresponds to *n* integrated US frames and *n* integrated PA frames. The number *n* is about 100 for the current setup, limited by the system memory. Data sets are acquired continuously; while one data set is being transferred, the next one is being acquired. We have optimized all parameters so that the transfer time is shorter than the acquisition time. This ensures continuous data acquisition and real-time imaging.

In such a continuous mode, the ultimate frame rate is governed by the mirror period. One mirror cycle lasts 24/720 Hz = 33.33 ms, which corresponds to a frame rate of 30 Hz for an integrated PAUS frame for a field of view of 2.8 × 2.8 cm (lateral × axial). Note that the laser scan range (~1 cm range) does not cover the whole PA image range. Nevertheless, because of light scattering inside tissue, it is almost homogeneous at a few millimeters depth and can cover the whole image range at the imaging depth (~1 cm). Both PA and US images were reconstructed using a delay-and-sum beamforming approach, Hilbert transformed, with the envelope displayed on a logarithm scale. A fusion image was also obtained by overlaying a PA image on the top of the corresponding US image (i.e., add PA pixel value to corresponding US pixel and display with different color mapping).

III. Results

A movie (played at 4 frames/s) shows all single-shot PA sub-images of the needle in the chicken breast over a complete scan cycle. The laser beam starts at the center (about 2 mm laterally) of the imaging range and swings to the right (8 mm laterally); it then goes to the left (−2 mm laterally) and finally goes back to the center. Fig. 4 shows snapshots of the movie for different laser positions, with Fig. 4(a): scan start at center, Fig. 4(b): right edge of the imaging area, and Fig. 4(c): scanning to the left side. The display dynamic range is 38 dB. Because of light scattering inside tissue, a large portion of the needle can be seen in each single-shot sub-image, not just a small section corresponding to the beam width (2.8 mm).

The results demonstrate that the SNR (>35 dB) is sufficient to easily visualize a needle at more than 1 cm depth using a single laser pulse with less than 2 mJ pulse energy for this configuration.

Fig. 5(a) shows the US image of the needle inside the chicken breast. The needle is slightly brighter than the tissue, with limited contrast because of background scattering. Note that before the needle was imaged, it was aligned with the image plane. This is why a trace from the alignment following the insertion path of the needle is seen in the region left of the needle tip. The needle is barely distinct from the trace in static US images.

In contrast to US, the integrated PA image, summed from single-shot sub-frames, exhibits more than 30 dB contrast over the background. The final PAUS fusion frame is shown in Fig. 5(b). The PA image is displayed in color and superimposed on the US image (gray scale). This image was also shown in the right panel of the scan-cycle movie at the end of one complete scan cycle. The US display dynamic range is 50 dB and that of the PA display is 35 dB. Two disconnected segments of the needle shown in the image correspond to the geometry and structure of the needle, with a tilted injection hole at the needle front. The top segment corresponds to the top edge of the needle, and the lower and shorter segment is the lower tip under the hole, with the proximal part not seen because light was blocked by the top needle edge. The rim of the hole has a weaker signal because it was away from the image plane in the elevational direction.

To fully mimic an interventional procedure using a needle, injection of an absorptive agent was imaged *ex vivo*. A movie (played at 16 frames/s) shows the process of an 18-gauge needle entering a piece of chicken breast, injecting ink solution, and exiting from the tissue. The movie contains four sections, corresponding to different operations: 1) Insert the needle from top right corner at an angle of about 20° to the lower left corner, with a maximum depth of 22 mm (12 mm below the tissue surface), creating a slim channel along the moving path. Fig. 6 shows several snapshots of the movie at this section; 2) Retract the needle until the tip stops at 18 mm in depth; 3) Inject the ink solution; and 4) Remove the needle. The images are displayed with a dynamic range of 50 dB for US and 35 dB for PA. Fig. 6 shows snapshots of the movie during needle insertion, with US-only images on the top row and combined PAUS images on the bottom row.

Snapshots of the movie during the injection process are shown in Fig. 7, with US-only images on the top row and combined PAUS images on the bottom row. The dynamic ranges of US and PA images are 50 dB and 35 dB, respectively. Right after injection, the needle tip is clearly seen in the PA image [Fig. 7(e)]. The small drop under the tip may be from leaking ink during the moving operation. Reverberation artifacts (i.e., multiple reflections) are also observed. In Fig. 7(f), more ink pours out and diffuses to the volume surrounding the tip. The ink then flows through the channel created when the needle was inserted [Figs. 7(g) and 7(h)]. at the end of injection, the diffused ink masks the needle tip, which is unseen [Fig. 7(h) and the remove section in the injection-cycle movie]. The injection process can be also seen in US images (Figs. 7a to 7d), although not clearly, with observations that tissue spreads from the channel because of the pressure of the injected ink solution, and small bubbles with shadow artifacts (the injection section in the injection-cycle movie). The

contrast of the needle/injected ink to the tissue background on the PA image is more than 30 dB with a laser penetration distance of more than 1 cm, demonstrating the feasibility of real-time PAUS image-guided drug delivery using the current scanning approach.

IV. Discussion

Integrated PAUS imaging for needle guidance has already been demonstrated in an *in vivo* model [31], [32]. However, the slow (<30 Hz) and bulky laser used in that study does not deliver frame rates appropriate for real-time monitoring, thus making clinical translation problematic. Here, we have demonstrated a system that can track a needle moving up to 1.2 cm depth in a chicken breast at a frame rate of 30 Hz. Given this rate, and the image quality presented in Figs. 5–7, integrated PAUS imaging may represent an attractive approach for needle guidance for applications (both percutaneous and transcutaneous) requiring a couple of centimeters of imaging depth.

A wavelength of 1053 nm was chosen in this study because it provides good penetration and high contrast among commonly used wavelengths (700 to 1100 nm) in PA imaging [33]. For needle guidance, the optical wave-length is not a critical issue because of the strong optical absorption in metals over the whole therapeutic range of wavelengths. In addition, inexpensive, compact, high-powered, fast commercial fiber or diode-pumped lasers operating at this wavelength are available, making clinical translation easier. Wavelength-tunable laser systems enabling spectroscopic imaging, such as the Opolette HR 532 (Opotek Inc., Carlsbad, CA) with length >60 cm including power unit + laser head, and versaScan OPO (Newport Corp., Irvine, CA) with length ~30 cm, are also available, and the scanning approach can be easily implemented using these laser systems. Compared with these laser systems, usually requiring an additional pumping laser, however, a single-wavelength system is still more compact. Additionally, techniques that can distinguish endogenous and exogenous absorbers in PA imaging at a single wavelength have been published [9], [34], [35]. For the particular example in [9], exogenous absorbers contain a magnetic component and thus can be magnetically manipulated. By detecting the magnetically-induced changes (e.g., displacement), exogenous absorbers can be differentiated from endogenous ones, which are insensitive to the magnetic field.

Although single-wavelength imaging in the region around 1 μm will have many applications, a robust PA molecular imaging system will require some level of wavelength tunability. A wavelength-tunable laser leveraging the same laser diode-pumped technology exploited here to serve as the pump for an OPO is a very real possibility for a system operating a high pulse repetition rates. We will explore this possibility in future work.

The laser scanning system presented here is not ideal for clinical translation. Optical delivery is at a large angle relative to the US imaging plane and free space optics is used for beam manipulation. A fiber-optic system must be integrated with the US array to produce an integrated PAUS probe. The beam can be distributed to a fiber bundle attached to both sides of a conventional US array to optimally illuminate the image plane [see Fig. 8(a)], similar to several designs already used in preclinical PAUS imaging systems [1]. Unlike these systems, however, the optical system must deliver the light to different fibers on each pulse to sweep

the small area beam coming from the high repetition-rate optical source. This could be achieved in a remote switching unit in which the laser output is injected to a different fiber on each laser pulse [see Fig. 8(b)]. We will design such a system as part of future work related to constructing a real-time PAUS imaging system based on the scanning-beam principles presented here.

In general, the narrow-beam scanning approach is equivalent to that using a broad-beam in terms of image quality when they have the same illumination area [16], [17]. The PA images are summed coherently, i.e., raw wave field after delay-and-sum beamforming but before Hilbert transformation. Because delay-and-sum is a linear operation, summing the wave field for each narrow laser beam is equivalent to the reconstructed wave field generated by a broad beam summed with all the narrow beams (Huygens–Fresnel principle). For imaging a fast-moving object, motion artifacts may be present. Nevertheless, no significant artifact should be observed because light is highly scattered at the imaging depth (~1 cm) and the illumination patterns from multiple beams overlap over the 1-cm scan range.

For needle guidance, the movement within one scan cycle (i.e., 33.33 ms) can be neglected for clinicians to monitor needle position, given a 30-Hz frame rate. In addition, the scanning approach gives much more flexibility in choosing the irradiation pattern when imaging objects with different geometries. The scanning trajectory can be chosen arbitrarily to meet a specific problem and to provide the maximum laser delivery to the target. The irradiation area is not limited by simple geometries, whereas for the wide beam illumination approach this can be a challenge. Applying image processing such as interpolation and weighting between narrow beam sub-images can further improve the SNR, and we will investigate such optimization schemes in future work.

The frame rate is currently limited by the laser average power regulation, 1 W/cm^2, as mentioned in the experimental setup section. To reach a frame rate larger than 30 Hz, the laser fluence must be smaller than 33.33 mJ/cm^2. For a higher frame rate, the fluence decreases and thus image SNR degrades. Nevertheless, with a high SNR (>35 dB for needle guidance), it is possible to increase the frame rate at the price of lower laser fluence (lower SNR), e.g., 50 Hz frame rate and 20 mJ/cm^2 fluence. Also, in the current setup, the mirror scans from one end to the other and returns within one cycle, so two full PA frames can be formed, instead of one. Therefore, with the setup unchanged, the frame rate can be doubled with the price of SNR degraded by 3 dB ($1/\sqrt{2}$). An alternate way is to scan in two dimensions with an additional galvo mirror to scan elavationally, in addition to lateral scanning, i.e., zigzag scan. The laser beam will not return to the same spot at each lateral scan cycle. The fluence can be kept constant while the laser PRF is increased and, thus, the frame rate increased. Optimizing the scan geometry to increase frame rate while maintaining a good SNR at the same time will also be part of our future work.

The unique mechanism of optical absorption-based contrast makes PA imaging an ideal modality for molecular imaging, while US can show simultaneous anatomical landmarks, providing context for molecular measurements [6], [7]. A particular example is to detect circulating tumor cells in blood vessels, providing a critical indicator of metastasis for cancer. As shown in our previous publications [8]–[10], metastatic tumor cells circulating in

the vasculature can be accumulated and detected using a composite nanosystem exhibiting both strong magnetic properties and high optical absorption at a desired wavelength. By targeting these particles to specific biomarkers on tumor cells, circulating tumor cells can be trapped and manipulated with an external magnetic system and non-invasively imaged using US-guided PA imaging. The imaging site is chosen at the radial artery in the forearm, which has a diameter of 1 to 2 mm and a level of 10 mL/min flow rate and, thus, a reasonable examination time to interrogate a significant blood volume. The accumulated cells create heterogeneous PA sources inside vessels, and thus can be detected by a commercial ultrasound probe with a narrow frequency band. In short, the system presented in this paper is well-suited to clinical translation of this technology.

The portable and low-cost laser used here operates at 1053 nm, within the optical window for biological tissue imaging [36]. The fluence distribution at 1053 nm near a radial artery in human forearm can be estimated using a Monte-Carlo simulation package (download available online [37] and described in [38]). We modeled the human forearm as a stack of layers (skin, fat, and muscle) and assumed the radial artery is located 6 mm away from the skin surface. Each layer was assumed to be flat with infinite lateral extension. At the maximum permitted exposure of laser irradiation at 1053 nm (100 mJ/cm^2) [15] with a Gaussian beam size of 2 mm diameter scanning over a 1-cm lateral extent with 21 laser beams, the fluence near the radial artery is more than 10 mJ/cm^2 (by superposition of all beams), sufficient for a good SNR PA imaging, comparable to that with a broad-beam, high-pulse-energy laser. For molecular imaging, a targeted contrast agent can be tuned to have strong optical absorption near 1053 nm. For example, clustered nano-structures have a significant red shift in their optical absorption spectra [39].

V. Conclusions

In this paper, we use a low cost, portable, and low-pulse-energy diode-pumped laser to generate PA signals. The final PA image is synthetically reconstructed by rapidly scanning a narrow-beam, low-pulse-energy laser across the imaging range. We have developed a portable and economical real-time, interleaved PAUS imaging system that provides real-time US and PA images at a frame rate of 30 Hz for an imaging area of 2.8 × 2.8 cm (lateral × axial). It is well-suited to 1 to 2 cm depth tissue imaging and provides a frame rate of 30 Hz that can be increased in the near future. The capabilities of this system were demonstrated by imaging needle insertion and subsequent agent injection. The target was located at more than 1 cm depth in light scattering tissue (a piece of chicken breast). Further system development, mostly in the laser delivery unit, can potentially enable a clinically translatable technology for real-time, integrated PAUS imaging.

Supplementary Material

Refer to Web version on PubMed Central for supplementary material.

Acknowledgments

This work was supported in part by the National Institutes of Health (NIH) RO1EB016034, R01CA170734, R01CA131797, R01CA140295, T32CA138312, the National Science Foundation (NSF) 0645080, and the Life Sciences Discovery Fund 3292512.

The authors give special thanks to P. Kaczkowski and R. Daigle at Verasonics in helping develop the scan sequence.

References

1. Wang, LV. Photoacoustic Imaging and Spectroscopy. Boca Raton, FL: CRC Press; 2009.
2. Li C, Wang LV. Photoacoustic tomography and sensing in biomedicine. Phys. Med. Biol. 2009; 54(19):R59–R97. [PubMed: 19724102]
3. Emelianov SY, Li P-C, O'Donnell M. Photoacoustics for molecular imaging and therapy. Phys. Today. 2009; 62(8):34–39. [PubMed: 20523758]
4. O'Donnell M, Wei C-W, Xia J, Pelivanov I, Jia C, Huang S-W, Hu X, Gao X. Can molecular imaging enable personalized diagnostics? An example using magnetomotive photoacoustic imaging. Ann. Biomed. Eng. 2013; 41(11):2237–2247. [PubMed: 23982280]
5. Niederhauser JJ, Jaeger M, Lemor R, Weber P, Frenz M. Combined ultrasound and optoacoustic system for real-time high contrast vascular imaging in vivo. IEEE Trans. Med. Imaging. 2005; 24(4):436–440. [PubMed: 15822801]
6. Wilson KE, Wang TY, Willmann JK. Acoustic and photoacoustic molecular imaging of cancer. J. Nucl. Med. 2013; 54(11):1851–1854. [PubMed: 24187042]
7. Homan KA, Souza M, Truby R, Luke GP, Green C, Vree-land E, Emelianov S. Silver nanoplate contrast agents for in vivo molecular photoacoustic imaging. ACS Nano. 2012; 6(1):641–650. [PubMed: 22188516]
8. Wei C-W, Xia J, Pelivanov I, Hu X, Gao X, O'Donnell M. Trapping and dynamic manipulation of polystyrene beads mimicking circulating tumor cells using targeted magnetic/photoacoustic contrast agents. J. Biomed. Opt. 2012; 17(10) art. no. 101517.
9. Hu X, Wei C-W, Xia J, Pelivanov I, O'Donnell M, Gao X. Trapping and photoacoustic detection of CTCs at the single cell per milliliter level with magneto-optical coupled nanoparticles. Small. 2013; 9(12):2046–2052. [PubMed: 23203788]
10. Wei C-W, Xia J, Pelivanov IM, Jia C, Huang S-W, Gao X, O'Donnell M. Magnetomotive photoacoustic imaging: In vitro studies of magnetic trapping with simultaneous photoacoustic detection of rare circulating tumor cells. J. Biophotonics. 2013; 6(6–7):513–522. [PubMed: 23420803]
11. Yang JM, Favazza C, Chen R, Yao J, Cai X, Maslov K, Zhou Q, Shung KK, Wang LV. Simultaneous functional photoacoustic and ultrasonic endoscopy of internal organs in vivo. Nat. Med. 2012; 18(8):1297–1302. [PubMed: 22797808]
12. Ke H, Erpelding TN, Jankovic L, Liu C, Wang LV. Performance characterization of an integrated ultrasound, photoacoustic, and thermoacoustic imaging system. J. Biomed. Opt. 2012; 17(5) art. no. 056010.
13. Alqasemi U, Li H, Aguirre A, Zhu Q. FPGA-based reconfigurable processor for ultrafast interlaced ultrasound and photoacoustic imaging. IEEE Trans. Ultrason. Ferroelectr. Freq. Control. 2012; 59(7):1344–1353. [PubMed: 22828830]
14. Dean J, Gornstein V, Burcher M, Jankovic L. Real-time photoacoustic data acquisition with Philips iU22 ultrasound scanner. Proc. SPIE. 2008; 6856 art. no. 685622.
15. American National Standard for Safe Use of Lasers in Health Care Facilities. 2007 Standard Z136.1–2000.
16. Xia J, Wei C-W, Pelivanov IM, O'Donnell M. Photoacoustic imaging using narrow beam scanning. IEEE Int. Ultrasonics Symp. 2011:2380–2383.
17. Xia J, Wei C-W, Huang L, Pelivanov IM, O'Donnell M. Comparison of PA imaging by narrow beam scanning and one-shot broad beam excitation. Proc. SPIE. 2011; 7899 art. no. 78991L.

18. Buehler A, Kacprowicz M, Taruttis A, Ntziachristos V. Real-time handheld multispectral optoacoustic imaging. Opt. Lett. 2013; 38(9):1404–1406. [PubMed: 23632499]
19. Razansky D, Buehler A, Ntziachristos V. Volumetric real-time multispectral optoacoustic tomography of biomarkers. Nat. Protoc. 2011; 6(8):1121–1129. [PubMed: 21738125]
20. Taruttis A, Morscher S, Burton NC, Razansky D, Ntzia-christos V. Fast multispectral optoacoustic tomography (MSOT) for dynamic imaging of pharmacokinetics and biodistribution in multiple organs. PLoS ONE. 2012; 7(1) art. no. e30491.
21. iThera Medical, Vision in reach: Clinical diagnostics. [Accessed Nov. 2014] 2012. [Online]. Available: http://www.ithera-medical.com/technology/clinical-systems.html,
22. Wang L, Maslov K, Xing W, Garcia-Uribe A, Wang LV. Video-rate functional photoacoustic microscopy at depths. J. Biomed. Opt. 2012; 17(10) art. no. 106007.
23. Zheng F, Zhang X, Chiu CT, Zhou BL, Shung KK, Zhang HF, Jiao S. Laser-scanning photoacoustic microscopy with ultrasonic phased array transducer. Biomed. Opt. Express. 2012; 3(11):2694–2699. [PubMed: 23162708]
24. Xi L, Sun J, Zhu Y, Wu L, Xie H, Jiang H. Photoacoustic imaging based on MEMS mirror scanning. Biomed. Opt. Express. 2010; 1(5):1278–1283. [PubMed: 21258548]
25. Montilla LG, Olafsson R, Bauer DR, Witte RS. Real-time photoacoustic and ultrasound imaging: A simple solution for clinical ultrasound systems with linear arrays. Phys. Med. Biol. 2013; 58(1):N1–N12. [PubMed: 23221479]
26. Kolkman RGM, Brands PJ, Steenbergen W, van Leeuwen TG. Real-time in vivo photoacoustic and ultrasound imaging. J. Biomed. Opt. 2008; 13(5) art. no. 050510.
27. Yuan J, Xu G, Yu Y, Zhou Y, Carson PL, Wang X, Liu X. Real-time photoacoustic and ultrasound dual-modality imaging system facilitated with graphics processing unit and code parallel optimization. J. Biomed. Opt. 2013; 18(8) art. no. 086001.
28. Natarajan S, Marks LS, Margolis DJ, Huang J, Macai-ran ML, lieu P, Fenster A. Clinical application of a 3D ultrasound-guided prostate biopsy system. Urol. Oncol. 2011; 29(3):334–342. [PubMed: 21555104]
29. Sauer G, Deissler H, Strunz K, Helms G, Remmel E, Koretz K, Terinde R, Kreienberg R. Ultrasound-guided large-core needle biopsies of breast lesions: Analysis of 962 cases to determine the number of samples for reliable tumour classification. Br. J. Cancer. 2005; 92(2):231–235. [PubMed: 15611793]
30. McMillan AM, Landorf KB, Gilheany MF, Bird AR, Morrow AD, Menz HB. Ultrasound guided corticosteroid injection for plantar fasciitis: Randomised controlled trial. BMJ. 2012 May 22.344 art. no. e3260.
31. Kim C, Erpelding TN, Maslov K, Jankovic L, Akers WJ, Song L, Achilefu S, Margenthaler JA, Pashley MD, Wang LV. Handheld array-based photoacoustic probe for guiding needle biopsy of sentinel lymph nodes. J. Biomed. Opt. 2010; 15(4) art. no. 046010.
32. Su J, Karpiouk A, Wang B, Emelianov S. Photoacoustic imaging of clinical metal needles in tissue. J. Biomed. Opt. 2010; 15(2) art. no. 021309.
33. Homan K, Kim S, Chen Y-S, Wang B, Mallidi S, Emelianov S. Prospects of molecular photoacoustic imaging at 1064 nm wavelength. Opt. Lett. 2010; 35(15):2663–2665. [PubMed: 20680092]
34. Huang S-W, Eary JF, Jia C, Huang L, Ashkenazi S, O'Donnell M. Diferential-absorption photoacoustic imaging. Opt. Lett. 2009; 34(16):2393–2395. [PubMed: 19684793]
35. Wei C-W, Lombardo M, Larson-Smith K, Pelivanov I, Perez C, Xia J, Matula T, Pozzo D, O'Donnell M. Nonlinear contrast enhancement in photoacoustic molecular imaging with gold nano-sphere encapsulated nanoemulsions. Appl. Phys. Lett. 2014; 104(3) art. no. 033701.
36. Tuchin, V. Handbook of Photonics in Biomedical Science. Boca Raton, FL: CRC Press; 2010. ch. 13.
37. Citations of MCML as of May 2009 [Online]. Available: http://oilab.seas.wustl.edu/mcmlcitations.html
38. Wang L, Jacques SL, Zheng L. MCML-Monte Carlo modeling of light transport in multi-layered tissues. Comput. Methods Programs Biomed. 1995; 47(2):131–146. [PubMed: 7587160]

39. Larson-Smith K, Pozzo DC. Pickering emulsions stabilized by nanoparticle surfactants. Langmuir. 2012; 28(32):11725–11732. [PubMed: 22823547]

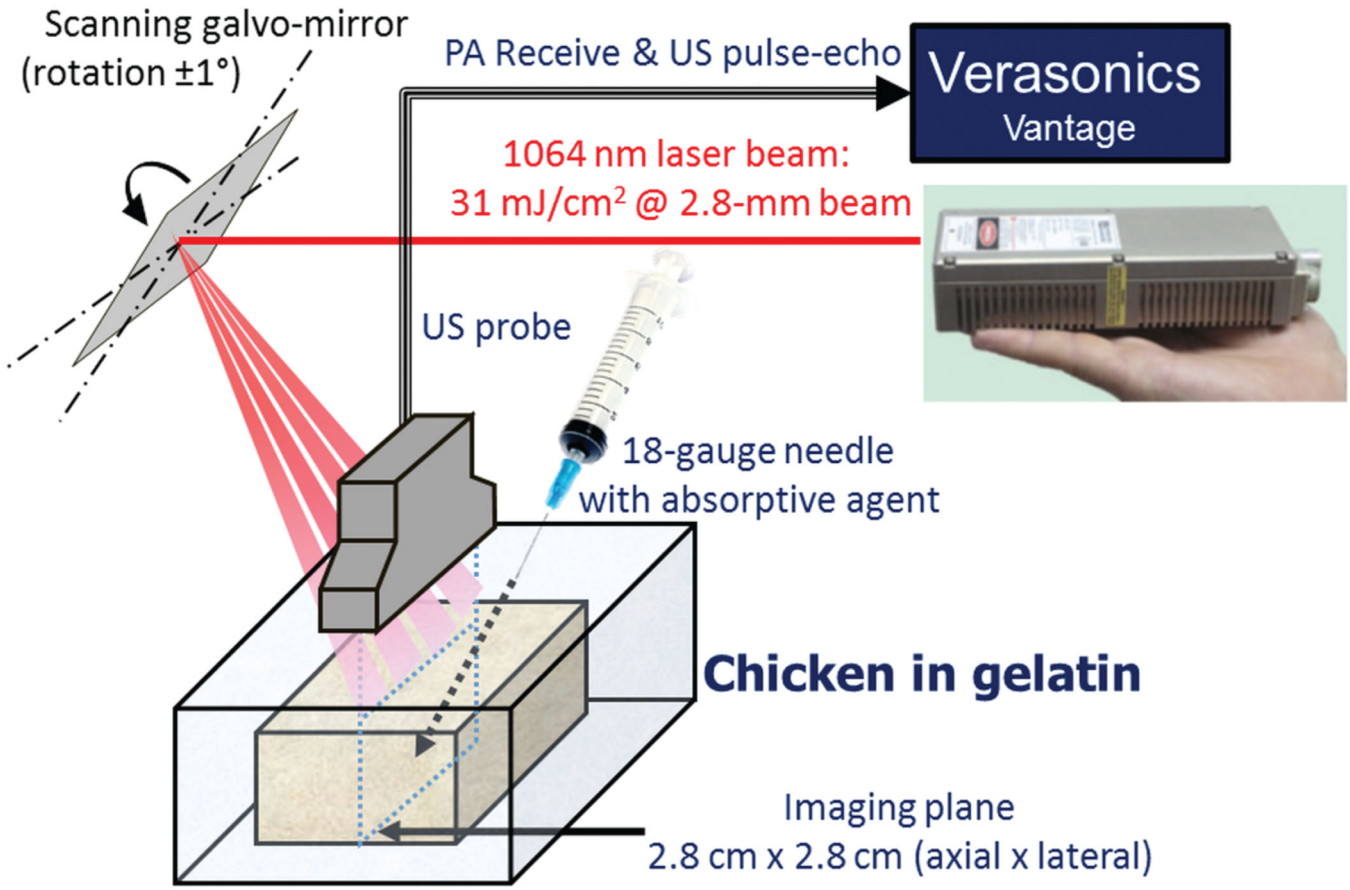

Fig. 1.

Schematic diagram of narrow laser beam scanning in the integrated PAUS imaging system used. A photograph of the laser used is shown, where a human hand serves to indicate scale.

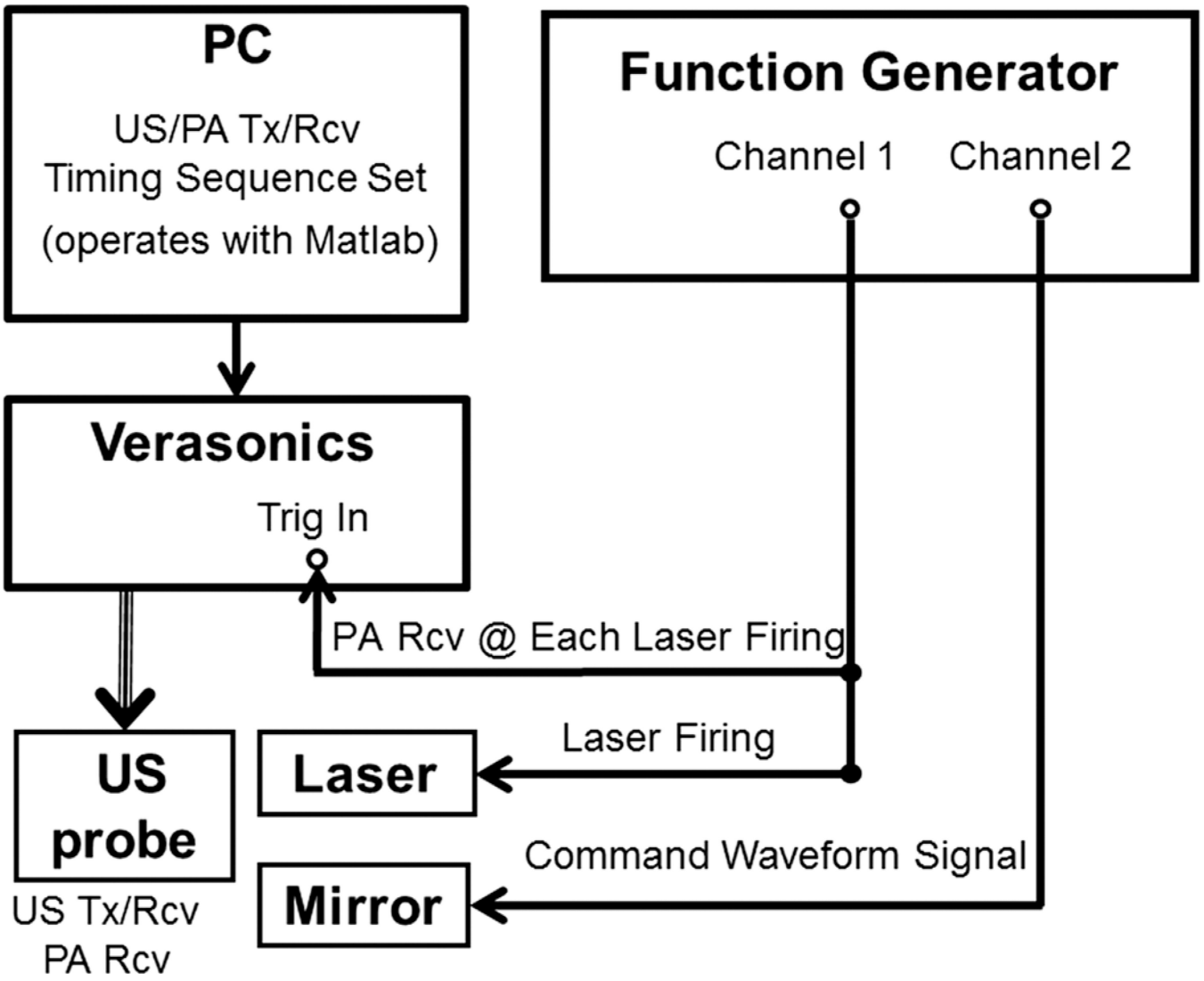

Fig. 2.

Experimental timing sequence control block. A Matlab program running on the Verasonics scanner regulates all US/PA transmits, receives, and data transfer events. The function generator synchronizes all events (laser firings, PA receives, and mirror positioning).

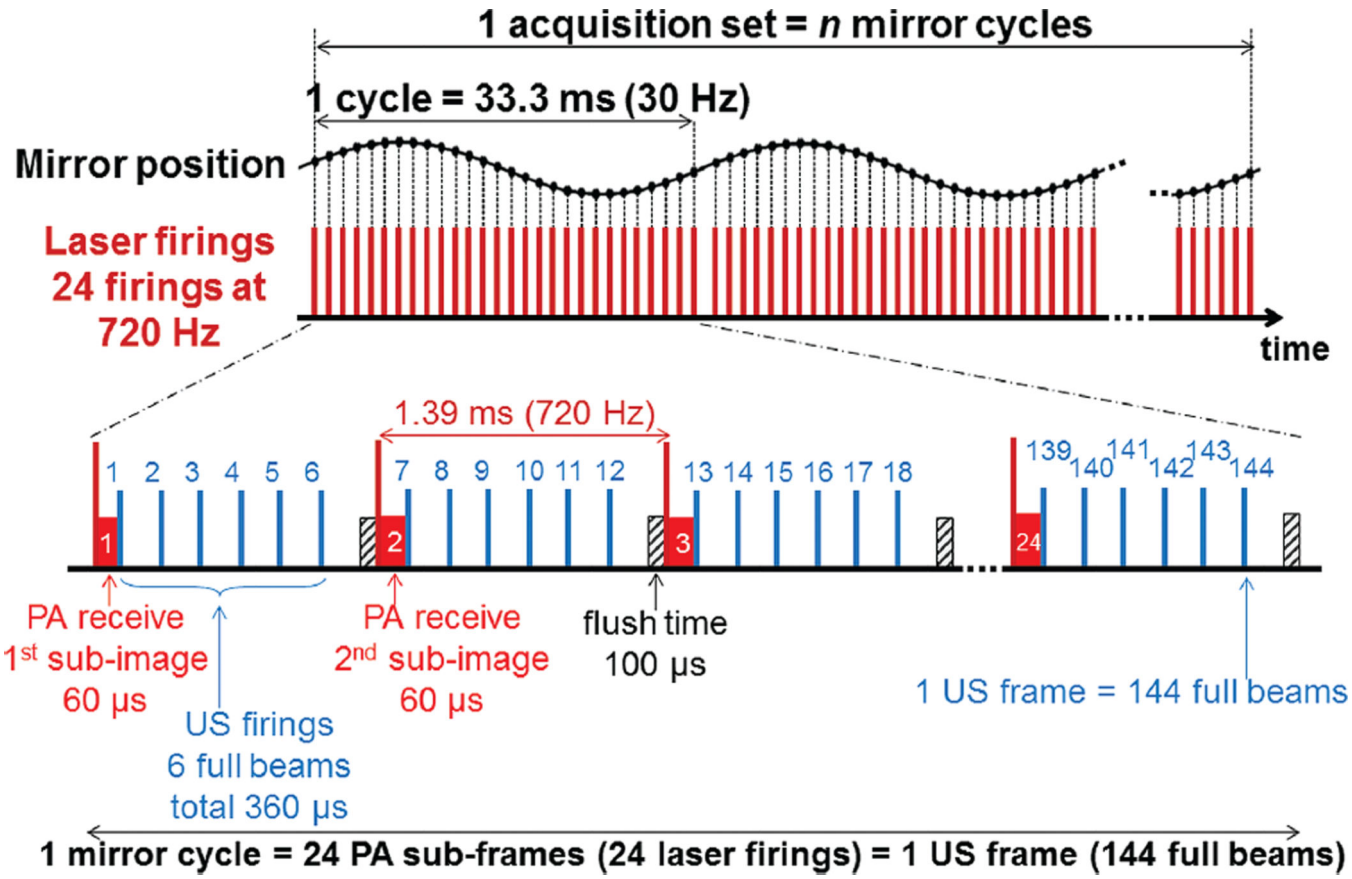

Fig. 3.

Detailed timing diagram for interleaved PAUS real-time imaging system. To achieve a 30 Hz real-time acquisition speed, acquired US/PA data are transferred and saved as a large data block unit in the Verasonics scanner. One acquisition set includes all saved data for *n* mirror scanning cycles. For each mirror cycle, there are 24 laser firings for PA data acquisition (128 channels for each laser firing). six US pulse–echo beams follow with 128 channels of parallel transmit and reception. As a result, one mirror cycle produces one PA frame with 24 sub-frames and one US frame from 144 beams, with a total integrated PAUS frame rate of 30 Hz.

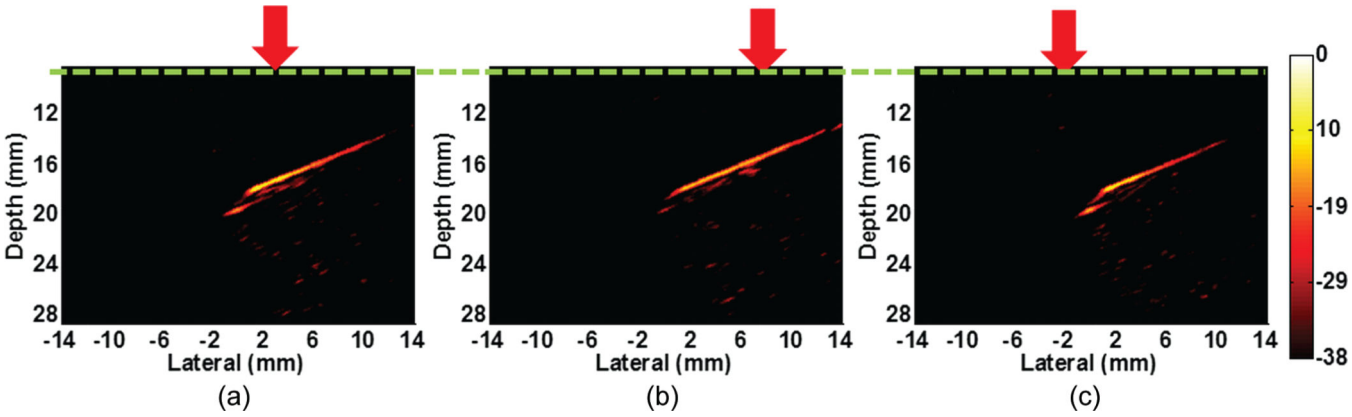

Fig. 4.

Single-shot PA sub-images of an 18-gauge needle in chicken breast with laser pulse at different scan positions. As the laser scans laterally, partial regions of the needle exhibit stronger signal compared with other parts for each single-shot sub-image. The laser scan range on the surface is about 1 cm with laser spot (a) at the center, (b) on the right edge, and (c) on the left side. The complete scan cycle takes 24 laser pulses (24 PA single-shot sub-images) at 720 Hz. The dashed line indicates the tissue surface. The display dynamic range is 38 dB. a movie (left panel) shows PA single-shot sub-images over a complete scan cycle. The acquisition rate is 720 sub-frames/s, but the movie is played at a slower rate (4 sub-frames/s) to show the scanning process.

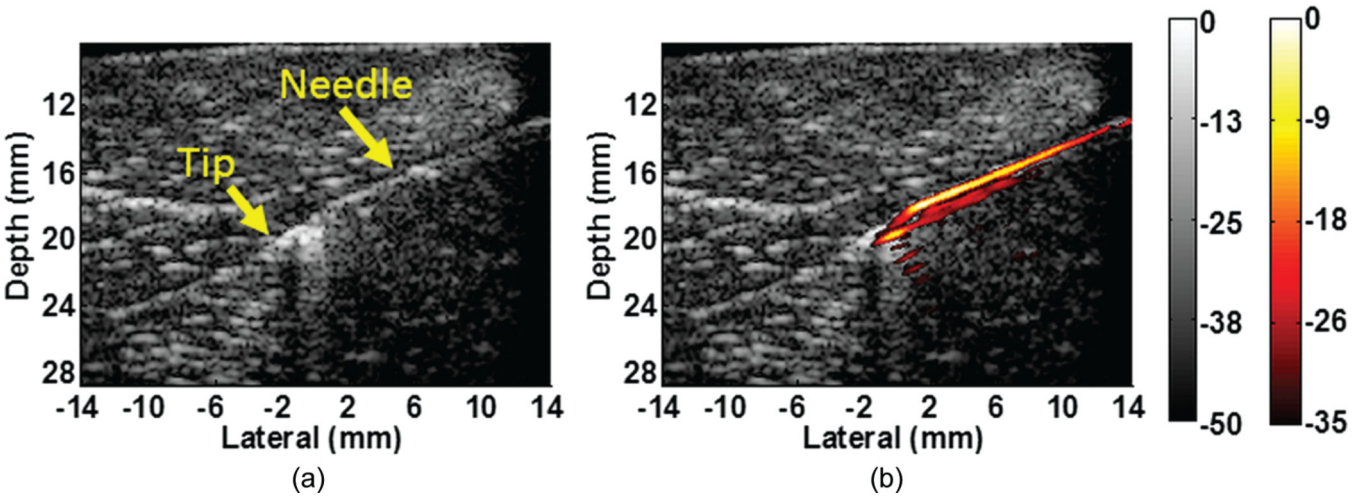

Fig. 5.

Ultrasound pulse-echo image (a) and fusion PAUS image (b) of the needle in chicken breast. The PA image is displayed on a color scale and superimposed on the gray-scale US image. The right panel of the scan-cycle movie shows a fusion PAUS image for 1 scan cycle. The display dynamic range is 35 dB for PA and 50 dB for US images.

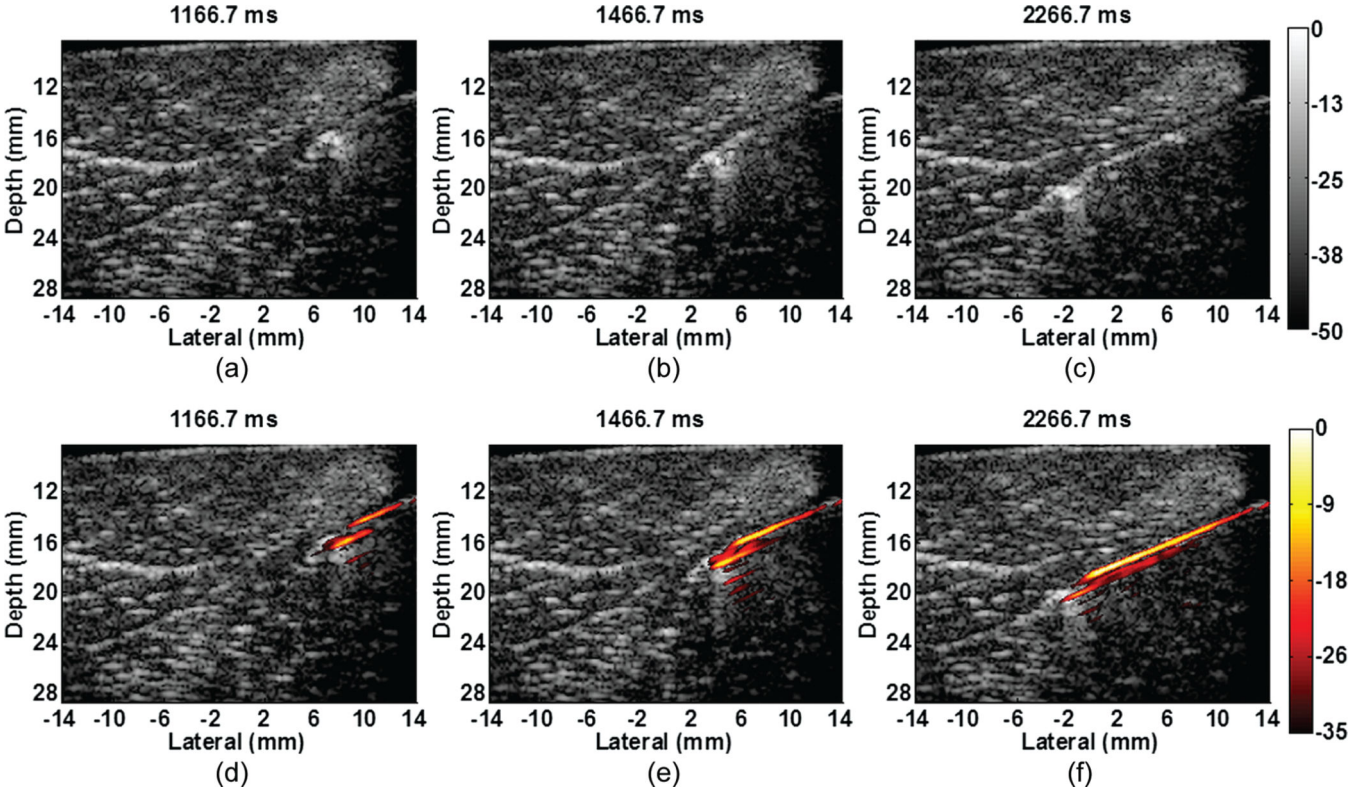

Fig. 6.

Snapshots of a movie (insert part) showing the insertion of an 18-gauge needle in chicken breast: (a)–(c) US images alone, and (d)–(f) combined US (gray scale)/PA (hot scale) images. The contrast of the needle to the background is more than 35 dB. The movie updates at 30 Hz (i.e., acquisition rate), corresponding to the scan rate of the galvo mirror, but is played at a slower rate (16 frames/s) to appropriately illustrate the process. The dynamic ranges of US and PA images are 50 dB and 35 dB, respectively.

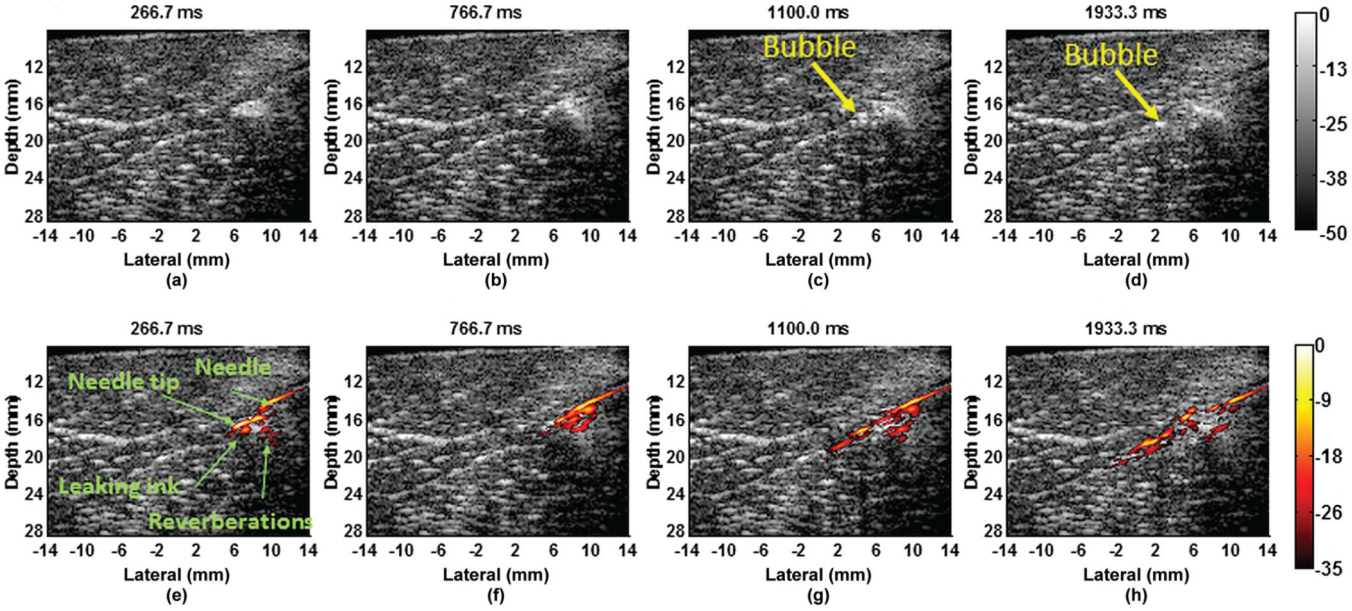

Fig. 7.

Snapshots of a movie (injection part) showing the injection of ink solution through the inserted needle in chicken breast: (a)–(d) US images alone, and (e)–(h) combined US (gray scale)/PA (hot scale) images. [(a) and (e)] Right after the injection started, [(b) and (f)] ink diffusing to the volume surrounding the needle tip, [(c) and (g)] ink flowing through the channel created during needle insertion, and [(d) and (h)] ink diffusing from the channel and masking the needle tip. The dynamic ranges of US and PA images are 50 dB and 35 dB, respectively. The movie has a real time update rate (i.e., acquisition rate) of 30 Hz, but is played at a slower rate of 16 frames/s.

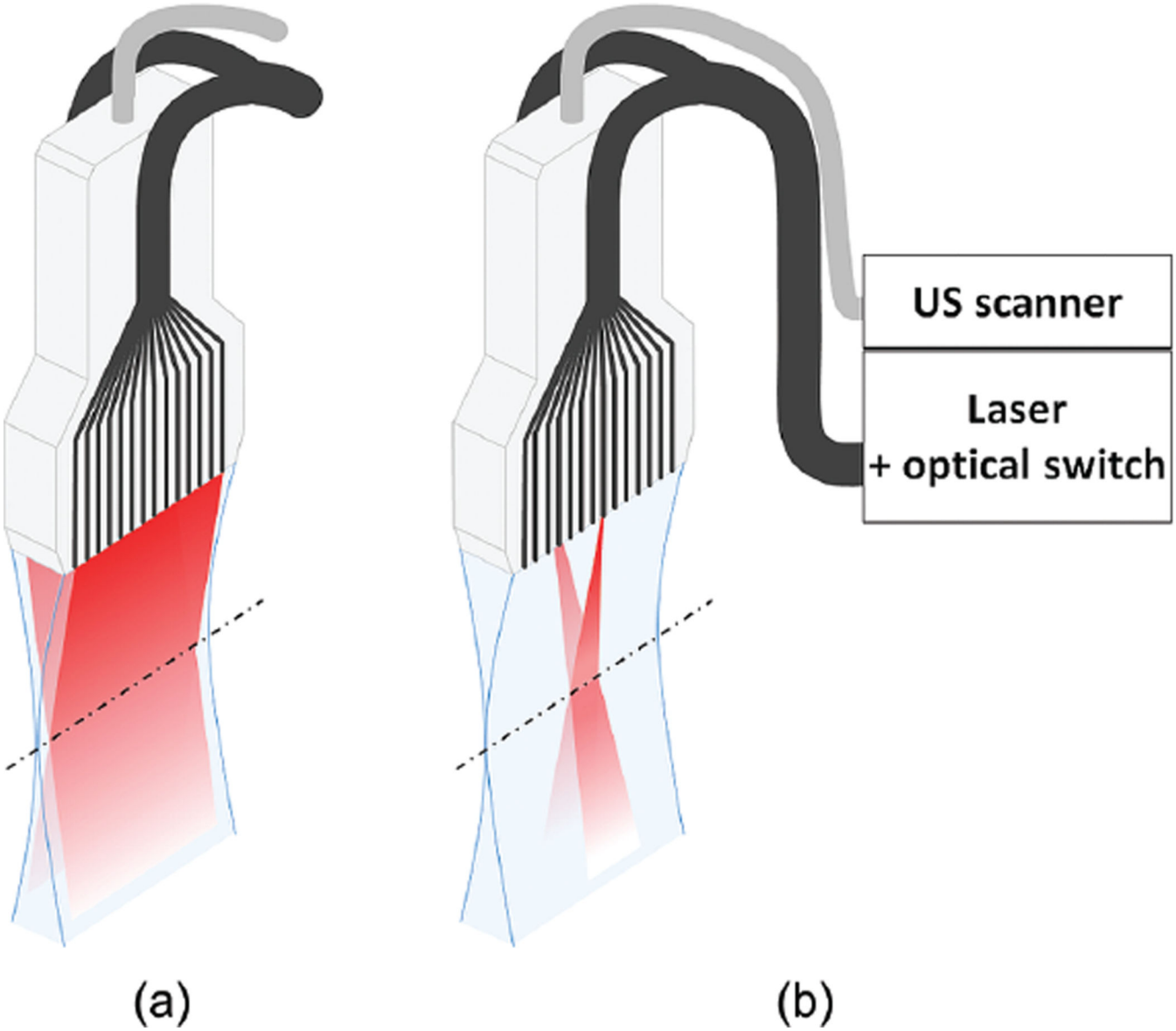

Fig. 8.

Proposed schematic diagram for an integrated PAUS probe. Multiple fibers are attached on both sides of an US linear array (i.e., on both sides of the elevation aperture). The US imaging area is represented in blue, and the illuminated area is represented in red. Fibers are arranged to deliver maximal pulse energy at the elevation focus of the US array (dash black line). (a) Standard wide-beam approach in which a large area is covered by illuminating all fibers simultaneously. (b) Narrow-beam scanning approach. The narrow beam issued from one fiber is swept across the imaging range using an optical switch that delivers light to different fibers at each pulse of a high-repetition rate laser.